Proceedings of the IASS 2024 Symposium
Redefining the Art of Structural Design
August 26-30, 2024, Zurich Switzerland
Philippe Block, Giulia Boller, Catherine DeWolf,
Jacqueline Pauli, Walter Kaufmann (eds.)

Experimental study on the In-Plane load-deflection behavior and wrinkling of highly inflated fabric arches

Runsheng Zhao, Xiongyan Li*, Xiaorui Liu, Wei Wang, Suduo Xue

* Faculty of Architecture, Civil And Transportation Engineering, Beijing University of Technology
Beijing 100124, PR China
xylee@bjut.edu.cn

Abstract

This study delves into the in-plane load-deflection and wrinkling response of highly inflated fabric arches. These structures, commonly utilized for temporary tents in both military and civilian settings, offer lightweight and portable solutions. By increasing the internal pressure, the load-bearing capacity of these structures can be significantly enhanced. Typically composed of composites, the membrane consists of a thermoplastic polyurethane (TPU) layer internally for airtightness and an external high-strength polyester braid to bolster tensile strength, enabling it to withstand high pressures. However, these materials are prone to wrinkling under heavy loads, reducing load-carrying capacity. Additionally, the structures exhibit significant geometric nonlinearities and are susceptible to large deformations. Through 12 sets of static loading tests on semicircular highly inflated fabric arches with varying spans and section diameters, this study elucidates the load-deflection behavior and wrinkling phenomenon. It highlights the importance of load-deflection curves and wrinkling load as crucial mechanical indicators, providing valuable insights into the structural behavior of high-pressure fabric arches.

Keywords: membrane, experiment, inflated fabric arch, load-deflection, wrinkle

1. Introduction

Inflatable membrane structures have emerged as a significant segment within contemporary architectural practices, owing to their intrinsic attributes of being lightweight, portable, and facilitating swift assembly and disassembly processes. These structures find extensive applications across diverse sectors including aerospace, military, industrial, and civil engineering [1],[2],[3]. Notably, the iconic Fuji Pavilion, conceived by Mamoru Kawaguchi, stands as a prominent testament to the architectural prowess of inflatable membrane structures [4]. Characterized by a central semicircular arch with outward protruding inflated arches at both ends, it exemplifies the innovative possibilities of such construction methodologies.

Furthermore, inflatable membrane structures serve as versatile shelters, prominently utilized in outdoor military operations and disaster relief efforts [5]. Leveraging the lightweight and flexible nature of membrane materials, coupled with the structural rigidity conferred by internal pressure, these structures effectively withstand external loads. Given the pivotal role of the inflatable arch as the primary load-bearing element, rigorous scrutiny is applied to its mechanical performance, underscoring the meticulous attention dedicated to ensuring structural integrity and reliability.

The inflatable arch, originally constructed from PVC material, faced limitations in membrane welds and material properties, restricting its internal pressure capacity to below 0.1MPa. Advancements led to the adoption of composite materials, featuring an inner bladder composed of TPU film and an outer layer of high-strength polyester fiber braid, allowing for internal pressures up to 0.75MPa.

Structural analysis of inflated membranes presents challenges addressed by various studies. Molly et al. [6] employed shell finite-element analysis to explore global buckling in fabric inflated arches under snow and wind loads. Davids [7] focused on in-plane load-deflection and buckling responses, developing a quadratic Timoshenko beam element. Malm et al. [8] conducted bending tests on airbeams under different inflation pressures to assess load-deformation behavior. Xue et al. [9] proposed a Pseudo Curved Beam (PCB) method for analyzing buckling behaviors, validated through bending experiments and numerical simulations of quarter-circle inflated arches.

The research landscape lacks comprehensive studies on the mechanical behavior of highly inflated fabric arches. This study filled this gap by conducting 12 sets of static loading tests on two highly inflated single arches of varying sizes. The objective was to investigate their mechanical responses under diverse stress conditions. By analyzing load-displacement curves at different internal pressures and load action modes, the study unveiled the deformation and fold development patterns of the structure under loading. The findings offer valuable empirical data for informing subsequent engineering design processes and facilitating accurate numerical simulations.

2. Experiment methodology

2.1. Specimen description

Two sets of highly pressurized fabric arches with varying specifications underwent bending tests. These arches comprised composite membrane material, featuring a dual-layer construction. The inner layer consisted of thermoplastic elastomer rubber (TPU) with a thickness of 1mm, while the outer layer was composed of high-strength polyester fiber, also 1mm thick. Circular looms were utilized to weave the fabric arches seamlessly into a singular structure, ensuring optimal performance under high internal pressure. The material for the arches was sourced from China Resources Textile Co., Ltd., based in Taizhou City, Jiangsu Province, with an operational pressure of 250kPa. Testing was conducted using a tiered pressure system: 250kPa, 200kPa, and 150kPa, respectively. To maintain air-tightness during testing, high-pressure air-tight interfaces were employed.

The specimens were circular in section, with arch A measuring 17800mm in length and having a section diameter of 300mm, while arch B had a length of 8400mm and a section diameter of 125mm. Both arches had restricted spans during testing, with arch A spanning 10200mm and arch B spanning 5200mm. Due to the multi-loading scheme of the test, the depths of the arches varied before each loading. Arch A had depths ranging from 6050mm to 6280mm, and arch B had depths ranging from 2553mm to 2633mm. The specific depths corresponding to each load case are detailed in Table 1.

The foundation of arch A comprised a sleeve frame, depicted in Fig. 1, where the arch feet were positioned within a circular sleeve matching the arch's section diameter. This arrangement served to restrict the rotation and displacement of the arch feet. To mitigate out-of-plane displacement induced by loading, polyester braided rope connected the arch's apex to the ground. Conversely, for arch B, with its smaller span and section diameter, the arch feet were secured to nearby structures to ensure stability. Similar out-of-plane restraints were implemented for arch B. Fig. 2 displays visual documentation of these structural components.

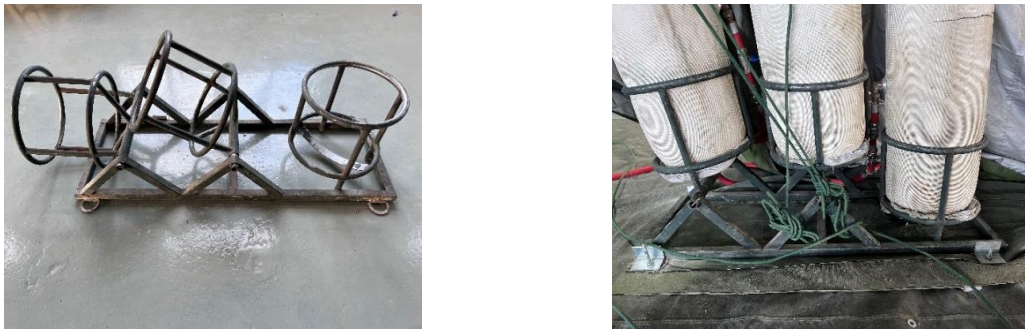

Figure 1: Steel sleeve frame

(a) (b)

Figure 2: Photograph of specimen: (a) Arch A, (b) Arch B.

2.2. Test setup and procedure

Currently, there are no established test standards for evaluating the structural performance of inflatable fabric members. In the absence of standardized procedures, tests were conducted on inflated fabric arches using single-point, two-point, and three-point bending methods to assess their load-displacement behavior. This testing approach involved a total of 12 sets of static loading to comprehensively evaluate the structural response of the arches.

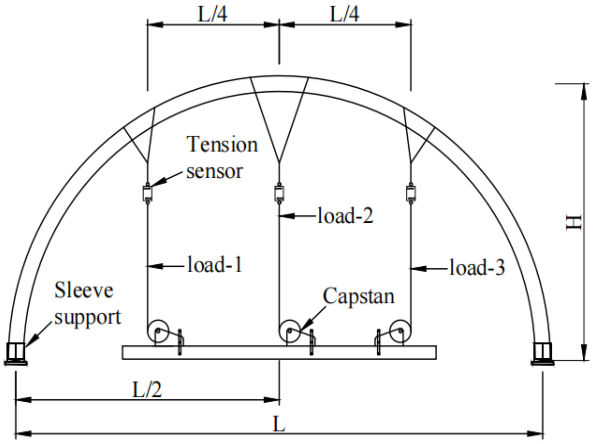

Figure 3: Test rig

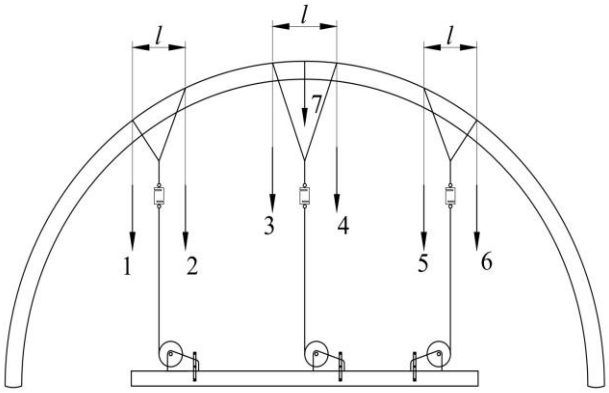

Figure 4: Schematic of the measurement points

To address the challenge of applying a significant concentrated load downward to the inflated membrane structure during testing, stay ropes were strategically wound along the arch axis adjacent to the loading point. This method distributed an equivalent surface load across the arch, mitigating local stress concentration. Arch A had a loading range of 300mm, while Arch B had 200mm. An upper rope connected to a lower hand winch, equipped with an S-type tension and pressure sensor (DSLY-103 500kg), facilitated the loading process. Each member featured three loading points, with Loading point-1 positioned at the mid-span and Loading points 2 and 3 at 1/4 of the span. Fig. 3 illustrates the setup for the bend test of the arches, and the schematic of the loading arrangement. The specific load cases for each test group are detailed in Table 1.

To prevent distortion of test results due to rapid loading, a graded loading system was implemented for both arch A and B. Initially, each level of arch A was loaded with 200N. Upon observing increased deformation, the load was reduced to 50N to accurately capture wrinkling load. Arch B began with a load of 100N at each level. Each level's load application time was controlled at 2 minutes, followed by a 10-minute waiting period after load application completion. Test data was recorded after deformation stabilization. Prior to each test set, members were depressurized and repressurized.

Table 1: Test parameter

Specimen	Load cases	Load point	Internal pressure/kPa	Rise of the arch/mm
Arch A	A-1	2	250	64300
	A-2	2	200	62450
	A-3	2	150	62000
	A-4	3	250	62100
	A-5	1, 2	250	62800
	A-6	1, 2, 3	250	62900
Arch B	B-1	2	250	2695
	B-2	2	200	2640
	B-3	2	150	2615
	B-4	3	250	2640
	B-5	1, 2	250	2642
	B-6	1, 2, 3	250	2625

2.3. Test method

The significant geometric nonlinearity of the membrane structure results in substantial deformation during loading, with varying load-displacement responses along the arch axis. To accurately characterize this deformation, seven symmetrically distributed displacement measurement points were established for each test member. These points were utilized for test data verification, ensuring the precision of the results. Fig. 4 illustrates the schematic diagram of these displacement measurement points.

At each measurement point, a 1m section of a tape measure was suspended to measure relative displacement during loading, aided by infrared readings. After unloading, the rebound displacement of the vault was recorded for each loading group. Additionally, a static strain testing and analysis system (Fig. 5 (a)) collected real-time tension values from sensors connected to a computer. Moreover, a high-precision digital pressure gauge (Fig. 5(b)) monitored pressure changes at the inflation port throughout the test.

(a) (b)

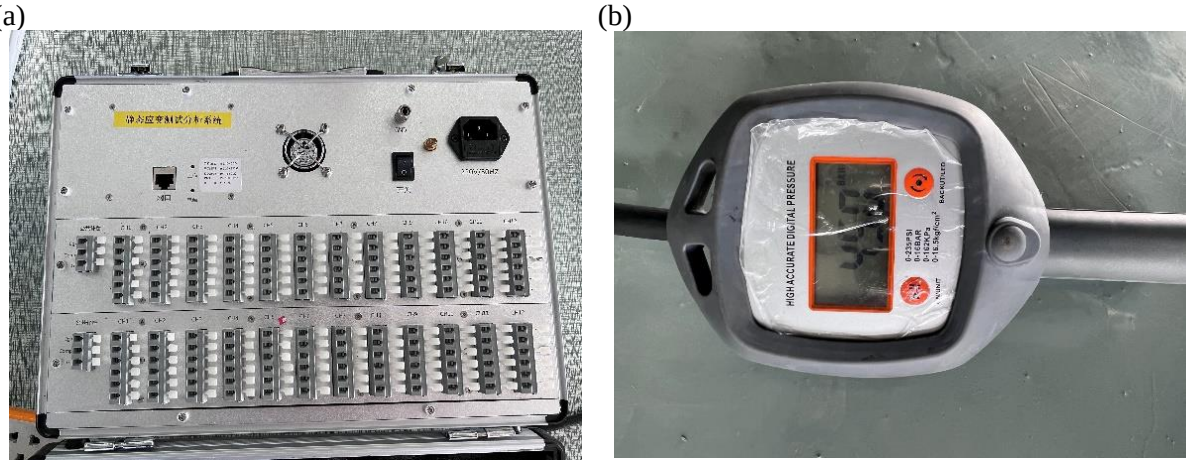

Figure 5: Measure equipment: (a) static strain testing and analysis system, (b) High-precision digital pressure gauge.

3. Experiment results and analysis

3.1. Arch A experiment results

3.1.1. Specimen A

The load-displacement data of the single-point loading mid-span measuring point (A-7) of arch A, which is shown in Fig. 6(a), illustrates its response to changes in loading position and internal pressure. At 250kPa internal pressure, the arch's deformation closely correlated with the loading position. Notably, bearing capacity improved significantly with a single point load at 1/4 span compared to the middle. Initially, the load-displacement curve exhibited a long linear stage. As the applied load reached 1145.13N, mid-span displacement increased significantly, indicating entry into a nonlinear stage. The arc segment between the loading point and mid-span gradually decreased, when the load reached 1426.19N, the arc segment of arch in this range approximately developed into linear beam. When subjected to a single point load at mid-span, the load-displacement curve exhibited a stronger nonlinear trend compared to loading at 1/4 of the span, leading to increased structural deformation. This phenomenon is attributed to the mid-span being the most critical section due to larger bending moments. Upon reaching the fifth load level of 962.36N, the structural vault's bending arc decreased, transitioning the loading area from "arc type" to "beam type," marking the onset of nonlinear behavior. As the load increased, the linear area expanded. By reaching 1426.88N, the vault displacement was 1135mm, and the mid-span area shifted from "upward convex" to "downward concave," accelerating structural deformation. Maximum deformation reached 1/10 of arch A's span, with no wrinkles observed on the membrane surface across all load cases, and the structure did not reach its ultimate load.

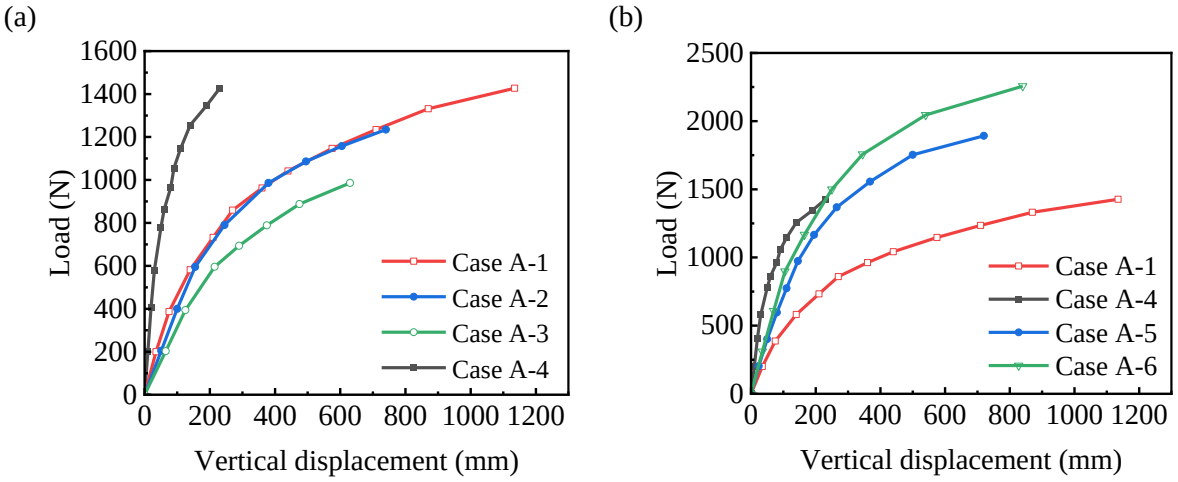

Figure 6: Bending test results of arch A: (a) single-point loading, (b) multi-point loading.

The load-displacement curve of the inflated arch under single-point loading showed less sensitivity to internal pressure during the linear stage. Under 200kPa and 250kPa internal pressure, there was no significant difference in the load-displacement response. However, with a drop to 150kPa, the component's stiffness notably decreased in the nonlinear stage, accompanied by a shorter linear stage in the load-displacement curve. At a load of 693.74N, under 150kPa internal pressure, the stiffness in the mid-span area of the arc section transitioned into a "straight line," distinct from the responses observed at 250kPa and 200kPa.

The load-displacement response of the inflated arch varied under different loading cases, as depicted in Fig. 6(b). When subjected to a 1/4-span single-point load, the structure exhibited maximum stiffness initially, but this stiffness gradually decreased as it entered the nonlinear stage. As deformation increased, the load-bearing capacity decreased, especially compared to multi-point loading cases. The arch showed the most significant nonlinear trend under mid-span single-point loading, with a lower load-bearing capacity. Under a three-point load, the mid-span arc section transitioned into a "straight line" at 2045.26N load and into a "concave shape" at 2256.35N load, with a gentler nonlinear phase development

compared to other cases. Load-displacement curves for 2-point loading and 1/4-span single-point loading exhibited similar trends, with relatively long linear ranges and similar structural deformations. Fig. 7 illustrates the structural deformation.

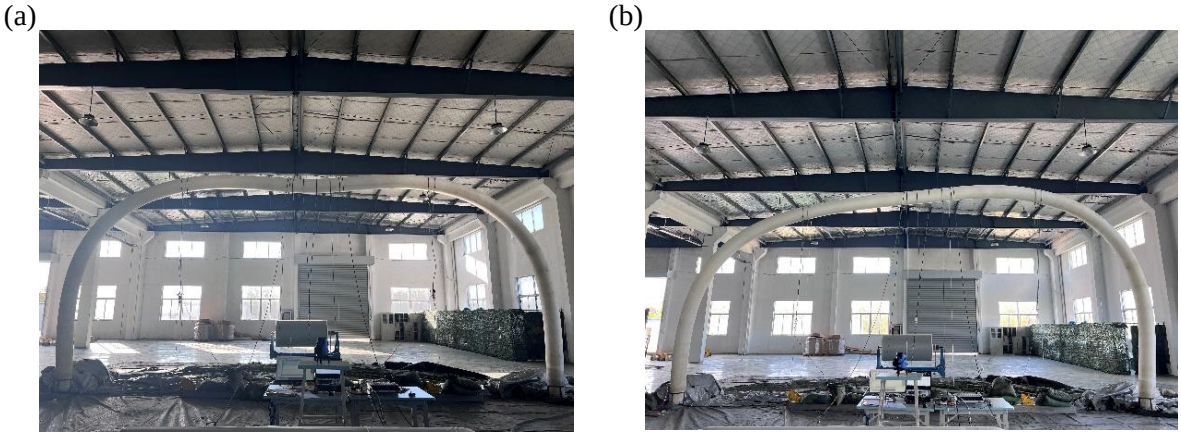

Figure 7: Structural deformation photo: (a) A-1, (b) A-5.

The load-displacement curves of each measurement point are depicted in Fig. 8. When subjected to both single-point and three-point loading across the span, the load-displacement curves of measurement points positioned symmetrically exhibited greater consistency. However, with three-point loading, variations in stiffness were observed among the three loading points, notably with reduced structural stiffness at the center of the span compared to other measurement points . Conversely, under two-point loading and quarter-span single-point loading casesconditions, the load-displacement curves at each measurement point displayed significant asymmetry .

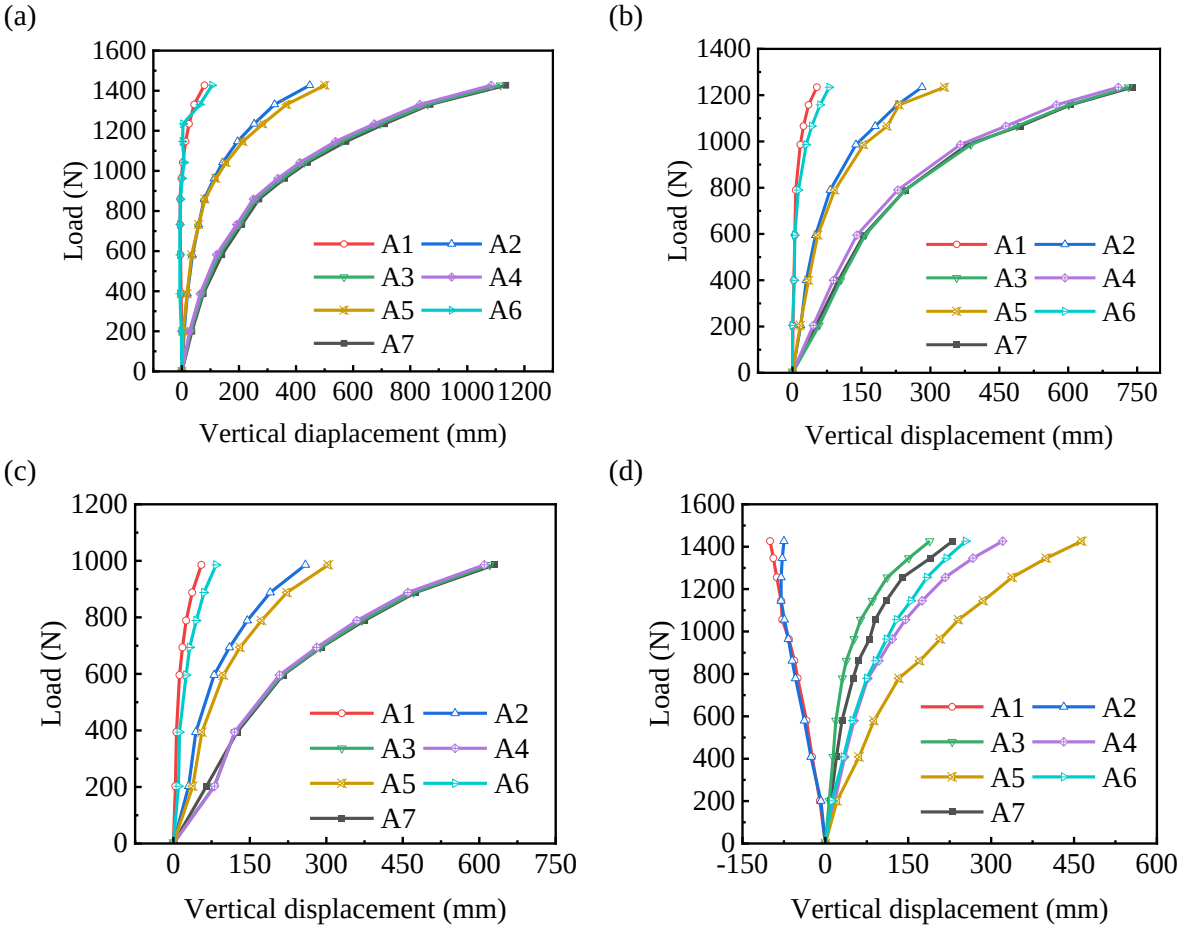

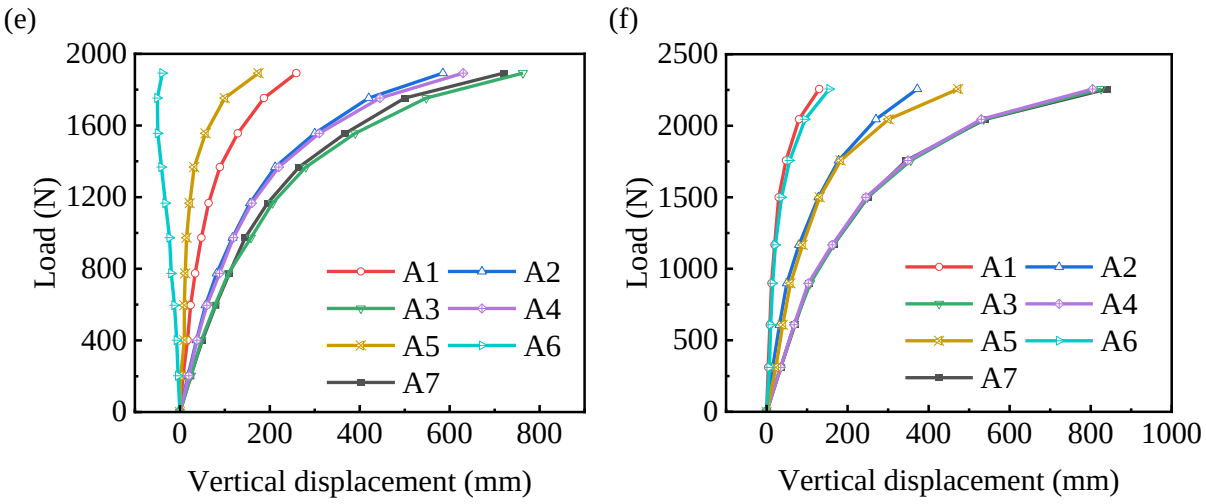

Figure 8: Bending test results of arch A: (a) Case A-1, (b) Case A-2, (c) Case A-3, (d)Case A-4, (e) Case A-5, (f) Case A-6.

3.1.2. Specimen B

Fig. 9(a) illustrates the load-displacement curves at the mid-span measurement point of arch B under single-point loading. Similarly to member A under an internal pressure of 250kPa, both measurement points exhibited maximum structural stiffness during 1/4 span single-point loading. However, the load-displacement curves for measurement point B displayed a more pronounced nonlinear trend, with the structure entering a nonlinear phase at a load of 254N. The loading region transitioned from a "straight line" to a stage of large deformation, attributed to the geometrical nonlinearity of the inflated arch. At a loading value of 393N, two fine-grained wrinkles emerged on the left shoulder of the arch (Fig. 10), with one wrinkle positioned 1660mm from the ground height and the other 1880mm from the ground, the loading area was developed from "straight line" to "concave shape". The emergence of the wrinkles was accompanied by the structural instability.

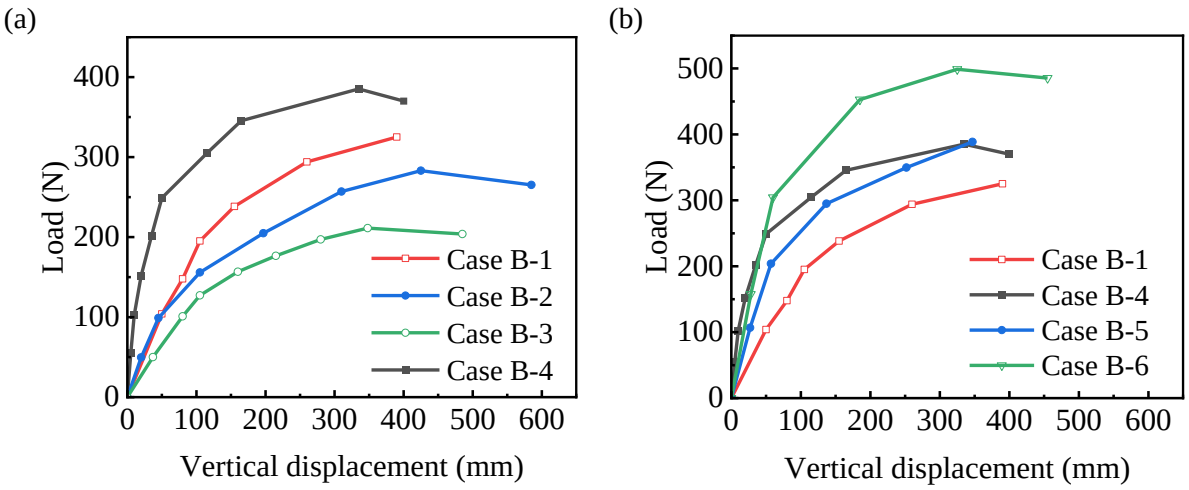

Figure 9: Bending test results of arch B: (a) single-point loading, (b) multi-point loading.

For member B, variations in internal pressure led to notable changes in the structure's load capacity. At internal pressures of 250kPa, 200kPa, and 150kPa, the corresponding wrinkled loads were 310N, 205N, and 160N, respectively. The buckling loads at these pressures were 325N, 275N, and 211N, respectively. Upon reaching the buckling load, the loading area transitioned from a "straight line" to a "concave type". At an internal pressure of 250kPa, the loading area shifted from an "arc type" to a "linear type", and entered into the stage of large deformation when loading to 243N, the corresponding load-displacement

curves also developed to the nonlinear stage. Continuing the loading to 310N resulted in wrinkles appearing on the membrane surface at 1660mm from the ground on the left side of the arch. These wrinkles gradually deepened, ultimately distributing on both sides of the arch in the form of fine lines.

(a) (b)

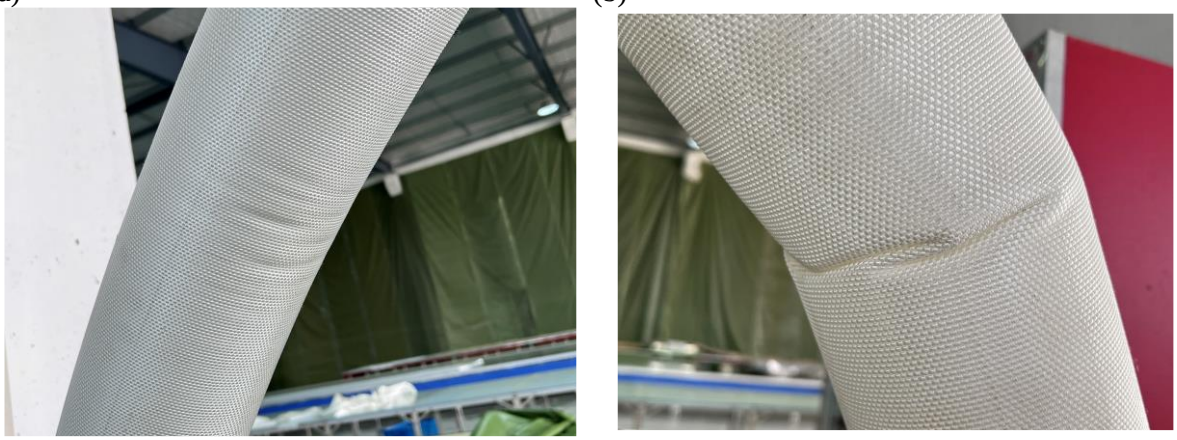

Figure 10: Wrinkling of specimen B during arch bend test: (a) Fine wrinkles, (b) Final form of wrinkle.

When the internal pressure was 200kPa, the loading area transitioned to a "linear" configuration, coinciding with the appearance of wrinkles. However, the structure had already entered the nonlinear stage due to significant deformation. Upon reaching the flexural load, a fine-grained wrinkle formed at the left shoulder of the arch, while the right shoulder developed a distinct wrinkle. Adjusting the internal pressure to 150kPa, wrinkles emerged on the left shoulder before the loading area became "linear". The generation of wrinkles preceded significant deformation. The load-displacement curve then entered a nonlinear stage dominated by wrinkles, with distinct wrinkles forming on each shoulder under flexural loading.

When the loading case of member B was changed, significant differences were observed in its load-displacement curves (as depicted in Fig. 9(b)). Under three-point loading, the structure exhibited a buckling load of 511N, entering a large deformation stage at 390N. At this point, the curvature of the arch decreased gradually, enhancing geometric nonlinearity. Upon reaching the buckling load, fine-grained wrinkles appeared at the left shoulder, and an obvious wrinkle formed at the right shoulder, while the loading area transitioned into a "straight line", and both members A and B had better ability to carry multi-point loads. For two-point loading, the buckling load was 388N, similar to 1/4-span single-point loading, but with lesser structural stiffness. The region between the loading points turned into a "straight line" at the buckling load, with a slight crease appearing at the left shoulder. Similar to member A, both members' load-carrying capacities were inferior when loaded at a single point in the span. Fig. 11 illustrates member B's load-displacement response at each measurement point.

(a) (b)

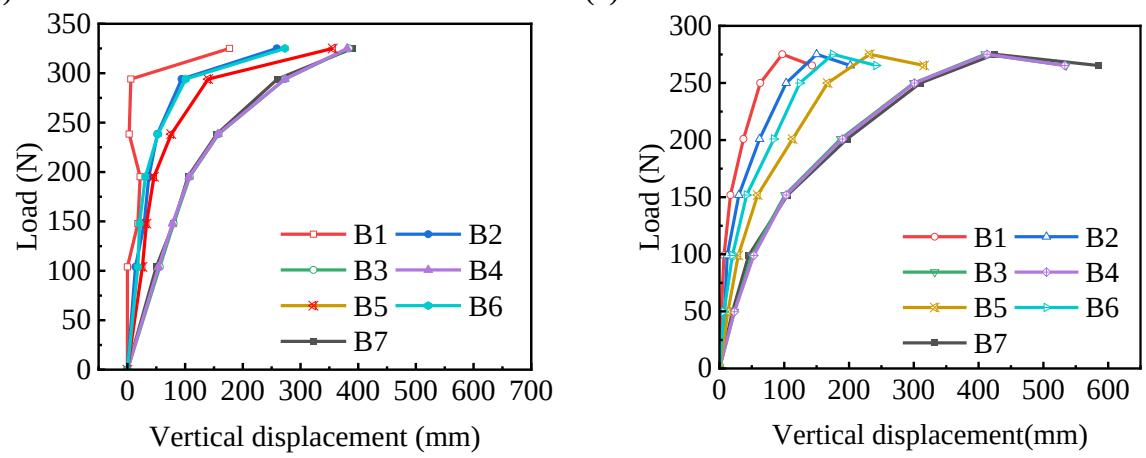

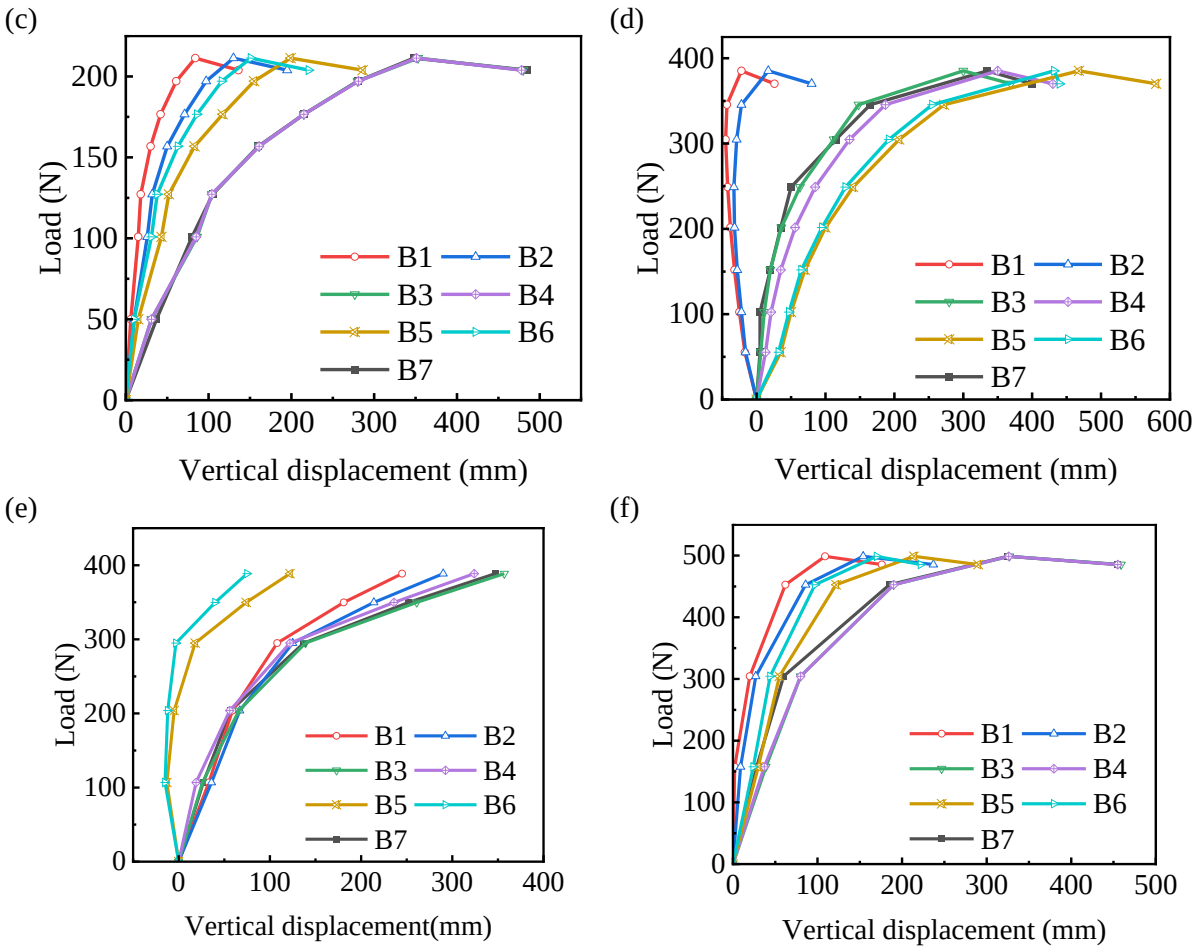

Figure 11: Bending test results of arch B: (a) Case B-1, (b) Case B-2, (c) Case B-3, (d)Case B-4, (e) Case B-5, (f) Case B-6.

3.2. Analysis and discussion

Comparing the test data for members A and B reveals several factors influencing the load-bearing capacity of inflated fabric arches:

1) Internal Pressure: Higher internal pressure correlates with increased load capacity.

2) Load Mode: Different loading modes impact load capacity differently.

3) Geometry: For smaller arches (member B), internal pressure primarily determines load capacity. Conversely, larger arches (member A) have a critical internal pressure threshold below which load capacity significantly decreases.

These findings highlight the complex interplay between internal pressure, load mode, and structural geometry in determining the load-bearing capacity of inflated fabric arch structures.

In the test, both members A and B exhibited significant deformations in the loading area, i.e, the loading area developed from "circular" to "straight" to "concave". However, member A did not show wrinkle formation after large deformation, attributing its reduced load-bearing capacity to structural geometric nonlinearity. In contrast, member B developed wrinkles influenced by internal pressure changes during large deformation. When comparing load-displacement responses under different loading modes, both members demonstrated strong load-bearing capacities under multi-point loading, with structural stiffness notably impacted by the loading mode.

4. Conclusion

In this paper, static tests under single-point, two-point and three-point loading were carried out on two kinds of highly inflated fabric arch with different spans and section diameters to quantitatively analyze the load-displacement response of arch under different loading cases. The conclusions are as follows:

(1) When the span of highly inflated fabric arch is less than 10m, internal pressure primarily influences the structural load-bearing capacity. Additionally, variations in internal pressure impact the development trend and final distribution state of wrinkles and large deformations. However, when the span exceeds 10m, increasing internal pressure does not significantly enhance the structural load-bearing capacity.

(2) Highly inflated fabric arches exhibit superior resistance to multi-point loads compared to single-point loads. Additionally, they demonstrate greater resilience to 1/4-span single-point loads than to single-point loads located at the midpoint of the span.

(3) With the increase of span and section diameter, the highly inflated fabric arch is less likely to be wrinkled, the form of structural instability is mostly due to severe deformation of the structural loaded parts, while the instability of the structure is caused by wrinkling when the arch span is small.

Acknowledgements

The research described in this paper was funded by the National Key Research and Development Program of China (No. 2023YFC3805600).

References

[1] J. P. Fay and C. R. Steele, “Bending and symmetric pinching of pressurized tubes,” International Journal of Solids and Structures, vol. 37, no. 46–47, pp. 6917–6931, Nov. 2000, doi: 10.1016/S0020-7683(99)00320-0.

[2] Z. Chen, H. T. Zhao, J. Chen, Z. T. Zhang, and D. P. Duan, “Deformation Analysis of the Tapered Inflatable Beam,” J. mech., vol. 34, no. 4, pp. 453–459, Aug. 2018, doi: 10.1017/jmech.2017.17.

[3] X. Wang, H. Fu, S. Law, Q. Yang, and N. Yang, “Experimental study on the interaction between inner air and enveloping membrane of inflated membrane tubes,” Engineering Structures, vol. 219, p. 110892, Sep. 2020, doi: 10.1016/j.engstruct.2020.110892.

[4] Q. Li, X. Guo, J. Gong, Q. Qing, and Z. Li, “Experimental deployment behavior of air-inflated fabric arches and a full-scale fabric arch frame,” Thin-Walled Structures, vol. 103, pp. 90–104, Jun. 2016, doi: 10.1016/j.tws.2016.02.005.

[5] W. G. Davids and H. Zhang, “Beam finite element for nonlinear analysis of pressurized fabric beam–columns,” *Engineering Structures*, vol. 30, no. 7, pp. 1969–1980, Jul. 2008, doi: 10.1016/j.engstruct.2007.12.020.

[6] S. J. Molloy, R. H. Plaut, and J.-Y. Kim, “Behavior of Pair of Leaning Arch-Shells under Snow and Wind Loads,” J. Eng. Mech., vol. 125, no. 6, pp. 663–667, Jun. 1999, doi: 10.1061/(ASCE)0733-9399(1999)125:6(663).

[7] W. G. Davids, “In-Plane Load-Deflection Behavior and Buckling of Pressurized Fabric Arches,” J. Struct. Eng., vol. 135, no. 11, pp. 1320–1329, Nov. 2009, doi: 10.1061/(ASCE)ST.1943-541X.0000068.

[8] C. G. Malm, W. G. Davids, M. L. Peterson, and A. W. Turner, “Experimental characterization and finite element analysis of inflated fabric beams,” Construction and Building Materials, vol. 23, no. 5, pp. 2027–2034, May 2009, doi: 10.1016/j.conbuildmat.2008.08.029.

[9] Z. M. Xue, C. G. Wang, J. T. Kang, and H. F. Tan, “Buckling analysis of an inflated arch including wrinkling based on Pseudo Curved Beam model,” Thin-Walled Structures, vol. 131, pp. 336–346, Oct. 2018, doi: 10.1016/j.tws.2018.06.044.